In Vivo Imaging of Natural Killer Cell Trafficking in Tumors

Filippo Galli[1,2], Anna Serafina Rapisarda[1], Helena Stabile[3], Gaurav Malviya[1,4], Isabella Manni[5], Elena Bonanno[6], Giulia Piaggio[5], Angela Gismondi[3], Angela Santoni[3], and Alberto Signore[1,2]

[1]Nuclear Medicine Unit, Faculty of Medicine and Psychology, Department of Medical-Surgical Sciences and of Translational Medicine, "Sapienza" University, Rome, Italy; [2]Department of Nuclear Medicine and Molecular Imaging, University Medical Center Groningen, University of Groningen, Groningen, The Netherlands; [3]Department of Molecular Medicine, "Sapienza" University, Rome, Italy; [4]Nuclear Medicine Unit, CRUK Beatson Institute, Glasgow, Scotland; [5]Molecular Oncogenesis Laboratory, Experimental Oncology Department, Regina Elena National Cancer Institute, Rome, Italy; and [6]Department of Biomedicine and Prevention, "Tor Vergata" University, Rome, Italy

Natural killer cells (NKs) are important effectors of the innate immune system, with marked antitumor activity. Imaging NK trafficking in vivo may be relevant to following up the efficacy of new therapeutic approaches aiming at increasing tumor-infiltrating NKs (TINKs). The specific aims of present study were to efficiently target NKs using a ^{99m}Tc-anti-CD56 and to image human NK trafficking in SCID mice bearing human cancer. **Methods:** The anti-CD56 monoclonal antibody (mAb) was radiolabeled with ^{99m}Tc, and in vitro quality controls were performed to test labeling efficiency, stability, and binding affinity to CD56. In vivo biodistribution was determined by injecting 5.5 MBq (104 ng) of radiolabeled antibody in the tail vein of SCID mice, which were then sacrificed at 1, 3, 6, and 24 h after injection. Targeting experiments were performed on 2 groups of SCID mice inoculated subcutaneously with increasing numbers of human NKs in the right thigh (from 2.5×10^6 to 40×10^6) and human granulocytes ($CD56^-$) or anaplastic thyroid cancer (ARO) cells in the contralateral thigh as control. TINK trafficking imaging was achieved by injecting 5.5 MBq of ^{99m}Tc-anti-CD56 mAb in SCID mice bearing ARO tumor xenografts in the right thigh, 24 h after being reconstituted with 10^5, 10^6, or 10^7 human NKs. **Results:** Anti-CD56 mAb was radiolabeled, achieving a radiochemical purity of more than 97% and a specific activity of 3,700 MBq/mg and retaining biochemical integrity and binding activity. In vivo studies revealed physiologic uptake in the liver and kidneys. Targeting experiments confirmed the specificity of labeled antibody to $CD56^+$ cells. Human NK cells injected in CD1 nude mice accumulated in the ARO tumors within 24 h and were imaged as early as 3 h after intravenous administration of ^{99m}Tc-anti-CD56. **Conclusion**: ^{99m}Tc-anti-CD56 is a promising tool for in vivo imaging of TINK cell trafficking.

Key Words: NK cells; anti-CD56; TINKs; imaging; nuclear medicine

J Nucl Med 2015; 56:1575–1580
DOI: 10.2967/jnumed.114.152918

Besides surgery, radiation, and chemotherapy, our own immune system has a key role against tumors. Recent scientific advances have demonstrated its importance and potential in oncology. Indeed, both innate and adaptive immunity cells are involved in the immune surveillance process that prevents tumor development either by releasing cytokines or by mediating a long-lived, antigen-specific response. However, such mechanisms are often inhibited by tumor cells capable of establishing a suitable microenvironment to sustain their proliferation (*1*).

In the last 20 years, many new therapeutic strategies aimed at increasing host response against tumors have been developed. These include cytokines, monoclonal antibodies (mAbs), vaccines, adoptive cell transfers, and Toll-like receptor agonists (*2–4*). In particular, natural killer cells (NKs) are a subset of lymphocyte with great cytotoxic potential. Approximately 90% of peripheral blood and spleen NKs are $CD56^{dim}CD16^+$ and possess high cytotoxic activity, whereas $CD56^{bright}CD16^-$ cells have mainly an immune-regulatory role (*5*). Under particular stimuli, NKs are able to kill certain targets, including tumor cells, even without any prior immunization. Interest in tumor-infiltrating NKs (TINKs) increased after publication of several studies that correlated the presence of NKs with tumor prognosis (*6*). High levels of TINKs are associated with good prognosis in patients affected by cancer (*7–9*). Given the importance of TINKs in the response against tumors, many companies are developing drugs that can increase the number and efficacy of TINKs.

In this context, imaging NK trafficking in vivo may be relevant to following up the efficacy of such novel therapeutic approaches. Several attempts to image NKs have been made in the past few years by different groups using direct labeling strategies that involve purifying cells from peripheral blood, radiolabeling with ^{111}In-oxine, and readministering to patients (*10,11*). This approach has limitations such as cell manipulation in culture and cell-function impairment after ex vivo labeling. Several studies reported that ^{111}In-oxine was toxic to cells, leading to improper migration into target organs (*12,13*).

Thus, we investigated a novel approach for in vivo cell labeling using a mAb that binds to CD56 antigen expressed on the surface of human NKs (*14*). The use of such a radiopharmaceutical may allow imaging of NKs directly in vivo, without the need for in vitro manipulation. The aims of present study were to efficiently radiolabel this mAb with ^{99m}Tc and to image human NK trafficking in SCID mice bearing human cancer.

MATERIALS AND METHODS

Antibody

The C218 hybridoma cell line (producing the anti-CD56 mAb) was kindly provided by Dr. A. Moretta (Institute Gaslini, Italy) (*15*). Hybridoma cells were cultured in RPMI medium supplemented with 5% fetal calf serum in a miniPERM bioreactor (Sarsted). After 8 d of

Received Dec. 16, 2014; revision accepted Jul. 9, 2015.
For correspondence or reprints contact: Alberto Signore, Nuclear Medicine Unit, St. Andrea Hospital, Via di Grottarossa 1035, 00189 Rome, Italy.
E-mail: alberto.signore@uniroma1.it
Published online Aug. 13, 2015.

culture, the medium was collected and clarified by centrifugation at 2,000 rpm for 10 min. The mAb was purified from hybridoma supernatant using protein-G–based affinity chromatography (Thermo-Scientific). The column was equilibrated with 10 volumes of binding buffer (0.1 M phosphate, 0.15 M NaCl) before the supernatant was loaded. Nonbound serum components were washed away with 10 volumes of binding buffer. The mAb was then eluted with 5 volumes of acidic elution buffer (glycine-HCl, 0.1 M; pH 2.7), and small fractions of solution that passed from the column were collected and subjected to spectrofluorimetric analysis. Fractions with an optical density of more than 0.1 at 280 nm were pooled and additionally purified through gel filtration, using a dextran desalting column (Thermo-Scientific).

Cell Lines and NK Purification

The anaplastic thyroid cancer cell line (ARO) was cultured in high-glucose Dulbecco modified Eagle medium (Gibco) supplemented with fetal calf serum, 10%; penicillin/streptomycin (penicillin G, 10,000 U, and streptomycin, 10 mg), 10 mL/L; amphotericin B (250 mg/mL), 10 mL/L; and L-glutamine, 1% (*16*). NKs were obtained from the blood of healthy donors. Healthy donors' peripheral blood mononuclear cells (4×10^5 cells) were isolated by Lymphoprep (Stemcell Technologies) gradient centrifugation and then cocultured for 10 d with irradiated (30 Gy) Epstein-Barr virus–transformed B-cell line RPMI 8866 (10^5 cells) at 37°C as previously described (*17,18*). After 10 d, the cells were collected and phenotypically characterized through immunofluorescence using anti-CD16 (3G8; BD-Biosciences), anti-CD56 (BD-Biosciences), and anti-CD3 (BD-Biosciences) mAb and analyzed by flow cytometry (BD-Biosciences). On day 10 the cell population was routinely greater than 90% $CD56^+CD16^+CD3^-$; when purity was less than 90%, contaminant T-cells were eliminated by immunomagnetic negative selection with anti-CD3 mAb to obtain a purity greater than 95%. Human granulocytes were isolated from healthy donors by Percoll (GE Healthcare) gradient centrifugation as previously described (*19*).

Labeling of Anti-CD56 mAb with ^{99m}Tc

Briefly, 1 mg of lyophilized mAb was resuspended in 500 μL of distilled water, and this solution was purified by size-exclusion chromatography using a G-25 Sephadex PD10 column (GE Healthcare) and nitrogen-purged phosphate-buffered saline (PBS) as eluent (20 mL). Indirect labeling of anti-CD56 mAb was performed by conjugation of the mAb with the heterobifunctional linker S-HYNIC (succinimidyl-6-hydrazinonicotinate hydrochloride) (SoluLink). The chelator (100 mM in dimethylformamide) was added at different molar ratios (from 20:1 to 50:1) to a solution of antibody (20 mM) in 100 mM sodium phosphate/150 mM NaCl buffer solution, pH 7.6–8.0. The mixture was purified by G-25 Sephadex PD10 column chromatography using nitrogen-purged cold PBS (pH 7.4) as eluent. The number of HYNIC groups bound per molecule of antibody was determined by molar substitution ratio assay. Briefly, 2 μL of conjugated anti-CD56 mAb were added to 18 μL of a 0.5 mM solution of 2-sulfobenzaldehyde in 0.1 M 2-(*N*-morpholino)ethanesulfonic acid buffer, pH 5.0, and incubated at room temperature for 2 h. After 2 h, the absorbance at 345 nm of each reaction was measured with a spectrophotometer and the number of HYNIC groups per molecule was calculated as indicated in the SoluLink data sheet. To efficiently label the mAb–S-HYNIC complex with ^{99m}Tc, to minimize the percentage of colloid formation, and to optimize the influence of the amount of coligand on the labeling efficiency, titrations of tricine (Sigma-Aldrich Chemicals; from 1 to 200 mg/mL in PBS) and $SnCl_2$ (Sigma-Aldrich Chemicals; from 1 to 10 mg/mL in 0.1 M HCl) were performed with mAb–HYNIC complex (25 μg) in 1 M sodium acetate (pH 5.5), using different amounts of freshly eluted $^{99m}TcO_4^-$ (100 μL) while keeping a constant reaction volume.

In Vitro Quality Controls of ^{99m}Tc-Anti-CD56 mAb

Quality controls were performed using instant thin-layer chromatography–silica gel strips (VWR International) as described elsewhere (*20*). The stability of the labeled antibody was measured in human serum and 0.9% NaCl solution at 37°C up to 24 h. For this purpose, 2 aliquots of 100 μL of ^{99m}Tc-anti-CD56 mAb were incubated with 900 μL of fresh human blood serum and with 900 μL of saline solution at 37°C. The percentages of free ^{99m}Tc and antibody-bound radioactivity were measured at 1, 3, 6, and 24 h by instant thin-layer chromatography–silica gel. In addition, a cysteine challenge assay was performed to check the in vitro stability of the radiolabeled antibody. ^{99m}Tc-anti-CD56 mAb was incubated at 37°C for 60 min at different cysteine:mAb molar ratios, which ranged from 500:1 at the highest cysteine concentration to zero in the absence of cysteine. At the end of the incubation time, each reaction mixture was evaluated by instant thin-layer chromatography–silica gel as described above. This experiment was repeated in triplicates. Possible modifications induced by the labeling procedure on anti-CD56 mAb were tested by sodium dodecyl sulphate–polyacrylamide gel electrophoresis under nonreducing conditions, according to the method of Laemmli (*21*). Proteins were visualized by staining the gels with Coomassie brilliant blue (Pierce). Radioactivity associated with each band was determined using a linear scanner (Bioscan Inc.). This experiment was performed after 3 different labelings.

Immunoreactive Fraction Assay

The immunoreactive fraction assay was performed using a constant concentration of radiolabeled mAb and serial dilutions of NKs according to a published method (*20*). Cells were washed 3 times in PBS and resuspended in a solution of cold 1% bovine serum albumin in PBS (BSA/PBS). Radiolabeled mAb at a constant concentration (50 ng/mL) in 1% BSA/PBS was added to different amounts of cells (final concentration ranging from 1×10^6 to 0.08×10^6 cells/mL) in triplicates with or without an excess of unlabeled antibody (100-fold molar excess). Cells were incubated for 2 h at 4°C and then washed twice with 500 μL of cold 1% BSA/PBS before cell-associated radioactivity was counted in a single-well γ counter (Gammatom). Data were plotted as a double inverse plot of the applied radiolabeled antibody over the specific binding, as a function of the inverse cell concentration. In this plot, the origin of the abscissa represents infinite cell concentration, that is, conditions of infinite antigen excess.

Uptake/Retention Assay (LigandTracer Assay)

Real-time measurements of cellular uptake and retention were performed 3 times after different labelings, using a rotating radioimmunoassay in a LigandTracer instrument (Ridgeview Instruments AB) (*22*).

In a typical experiment, $CD56^+$ NKs (5×10^6) are resuspended in 1 mL of PBS and plated into fibronectin-coated plastic circular Petri dishes and activated with 0.20 M *N*-ethyl-*N*′-(dimethylaminopropyl) carbodiimide and 0.05 M *N*-hydroxysuccinimide. Each dish is then incubated with cells and placed in the LigandTracer during a continuous rotation of 1 h, to allow release of weakly attached cells. After a single gentle wash, the cell dish is ready for measurement. Radiolabeled mAb (0.7 nM) in pH 7.4 PBS supplemented with 7% cell culture medium devoid of fetal calf serum is then added.

When the radiolabeled antibody binds to the cells, a detector placed over the elevated part of the dish registers the cell-bound activity each time the cells pass through the detector. By following the activity over time, a real-time binding curve is obtained, using LigandTracer software, version 1.1. Data are exported and analyzed with GraphPad software to determine the dissociation constant.

In Vivo Biodistribution and Cell Targeting

For animal experiments, the institutional and national guide for the care and use of laboratory animals was followed. For in vivo biodistribution studies, 5.5 MBq (100 μL) of labeled anti-CD56 were injected in the tail vein of 12 SCID mice and static planar posterior

images were acquired using a high-resolution portable mini γ camera (*23*) at 1, 3, 6, and 24 h under light ether anesthesia. At the end of each imaging point, 3 mice were sacrificed and major organs were collected and counted in a single-well γ counter. Time–activity curves in organs were created for both in vitro and ex vivo data. For cell-targeting studies, 2 groups of 24 SCID mice were subcutaneously injected in the right thigh with increasing numbers (from 2.5×10^6 to 40×10^6) of human $CD56^+$ NKs mixed with Matrigel (BD-Biosciences). In the contralateral thigh of both groups, $CD56^-$ cells (ARO or human granulocytes) were injected as a negative control. After 1 h, 5.5 MBq of ^{99m}Tc-anti-CD56 were injected in the tail vein and planar posterior images were acquired at 1, 3, 6, and 24 h.

Kinetic Studies of NK Infiltration in Tumors

To investigate the kinetics of NK infiltration in our xenograft model, ARO cells from a male donor (XY genotype) mixed with Matrigel were injected subcutaneously in the right thigh of 18 male SCID mice (XY genotype). After tumor growth, 10^6 NKs from a female donor (XX genotype) were injected in the tail vein. After 3 h, 3 mice were sacrificed and tumors were collected, formalin-fixed, and paraffin-embedded. The same procedure was repeated at 6, 12, 24, 48, and 72 h. Histologic analysis were performed at each time point, including hematoxylin and eosin staining of sections, immunohistochemistry, and fluorescent in situ hybridization (FISH) for the Y chromosome, allowing us to differentiate exogenous human TINKs (XX genotype) from endogenous TINKs and ARO cells (XY genotype). Immunoperoxidase staining with an anti-CD57 mAb—revealed with DAB after a secondary antibody incubation—was performed to identify $CD57^+$ TINKs. CD57 was chosen as an NK marker to avoid any interference from injected anti-CD56.

Imaging of TINKs in SCID Mice with ARO Tumors

Imaging of exogenous human TINKs was performed on 4 groups of SCID mice ($n = 12$) bearing an ARO tumor xenograft in the right thigh. Three groups received 10^5, 10^6, and 10^7 human NKs, whereas the fourth group was used as a negative control. After 24 h (as determined from previous experiments), 5.5 MBq of ^{99m}Tc-anti-CD56 were injected in the tail vein of each mouse, and planar posterior images were acquired by a high-resolution portable mini γ camera at 1, 3, 6, and 24 h after injection. After the last time point, the mice were sacrificed for organ counting and histology.

RESULTS

Labeling and Quality Control of Anti-CD56 mAb

Molar substitution ratio analysis of HYNIC-conjugated mAb revealed the presence of 9.1, 18, and 23.5 molecules of chelator per molecule of antibody, when conjugated with a 20:1, 30:1, and 50:1 HYNIC:mAb ratio, respectively. A ratio of 30:1 was selected as the formulation of choice since no modification of binding activity was observed. Optimization of ^{99m}Tc labeling of HYNIC–mAb conjugate (25 μg of mAb; 30:1 HYNIC:mAb ratio; tricine, 55.8 mM; $SnCl_2$, 170 μM; 92 MBq; 10-min incubation at room temperature) gave a radiochemical purity of more than 97% after purification by size-exclusion chromatography. The specific activity was 3,700 MBq/mg. Radiolabeled anti-CD56 mAb was stable in both saline and human serum up to 24 h (>90%). The cysteine challenge assay demonstrated moderate stability up to a 200-fold molar excess of cysteine (supplemental data, available at http://jnm.snmjournals.org). Sodium dodecyl sulphate–polyacrylamide gel electrophoresis analysis showed no significant differences between the native and radiolabeled anti-CD56 mAb (supplemental data). Native, conjugated, and radiolabeled mAb showed a band of approximately 150 kDa (i.e., molecular weight of complete mAb). However, a small band of more than 250 kDa was also present in both lanes and could be ascribed to dimers of the complete mAb, but the radioactivity was associated only with the band corresponding to the intact mAb.

In Vitro Binding Experiments

The immunoreactive fraction assay data demonstrated a closely linear relationship of total applied/specific binding as a function of the inverse cell concentration. Unspecific binding was negligible, and 76.9% (SD = ±3.5, SEM = 1.73) of the radiolabeled mAb was immunoreactive (Fig. 1). LigandTracer experiments showed that the radiolabeled mAb was able to bind to NKs over time, reaching a plateau at between 1 and 2 h. After replacement of the radioactive medium with PBS, ^{99m}Tc-anti-CD56 was strongly retained on the cell surface, with a slow off-rate (Fig. 2). A dissociation constant of 1.7×10^{-10} (SD = $\pm 0.02 \times 10^{-10}$, SEM = 0.0153×10^{-10}) was calculated by averaging 3 different experiments. At the end of these experiments, all cells were viable (as assessed by trypan blue exclusion), thus indicating that at least until 33 h the ^{99m}Tc-mAb was not toxic to NKs.

In Vivo Biodistribution and Cell Targeting

In vivo biodistribution studies, summarized in Figure 3A, showed a high circulating activity up to 24 h, with uptake occurring predominantly in the liver and, to a lesser extent, in the kidney. Blood and liver showed the highest percentage injected dose per gram at 1 h, whereas at 24 h the highest activity was detected in the spleen (Fig. 3A). Cell-targeting experiments demonstrated the possibility of imaging as little as 2.5×10^6 NKs in a volume of 300 μL, with a target-to-background (T/B) ratio of 1.8 (SD = ±0.1, SEM = 0.0577) at 24 h. Animals injected with more than 10^7 NKs showed a T/B ratio up to 4 at 24 h (Fig. 4).

Kinetic Studies of NK Cell Infiltration in Tumors

Studies of NK kinetics in vivo demonstrated that they were able to infiltrate tumors as early as 3 h after injection, with a slight increment over time and no contamination of host NKs as shown by FISH analysis (Fig. 5; supplemental data). The most severe infiltration was between 12 and 24 h, whereas after 24 h the tumor started to show necrotic areas induced by NK killing of tumor

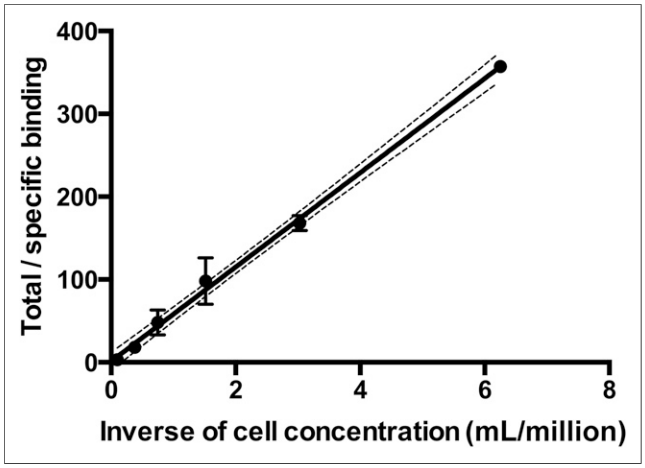

FIGURE 1. Double inverse plot of data obtained by immunoreactive fraction assay of radiolabeled ^{99m}Tc-anti-CD56 mAb. Each point represents mean of 3 different experiments, and error bars represent SD ($y = 56.88x + 1.33$; $R^2 = 0.997$).

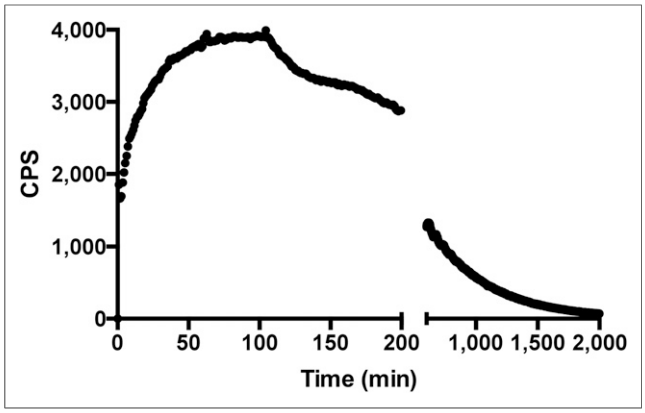

FIGURE 2. Binding trace graph (decay-corrected) for uptake of ^{99m}Tc-anti-CD56 mAb to human NKs in vitro reaching maximum binding after 60 min. At this time point, radioactive medium was replaced with cold PBS and retention studies were performed. Each point represents single measurement on same petri dish over time.

cells. We therefore selected 24 h as best time point for future experiments.

Imaging of TINKs in SCID Mice with Implanted ARO Tumors

The radiopharmaceutical allowed clear visualization of tumor xenografts with almost no signal from negative controls. The highest uptake was detected at 24 h after injection, with a T/B ratio of 6.02 that correlated with the number of $CD56^+/CD57^+$ TINKs as confirmed by immunohistochemistry studies (Fig. 6). Moreover, the number of NKs positively correlated with the size of the tumors ($r^2 = 0.89$; $P = 0.001$) and with the radioactivity detected by ex vivo organ counting ($r^2 = 0.90$; $P = 0.001$) (Fig. 7). No correlation was found between the number of injected NK

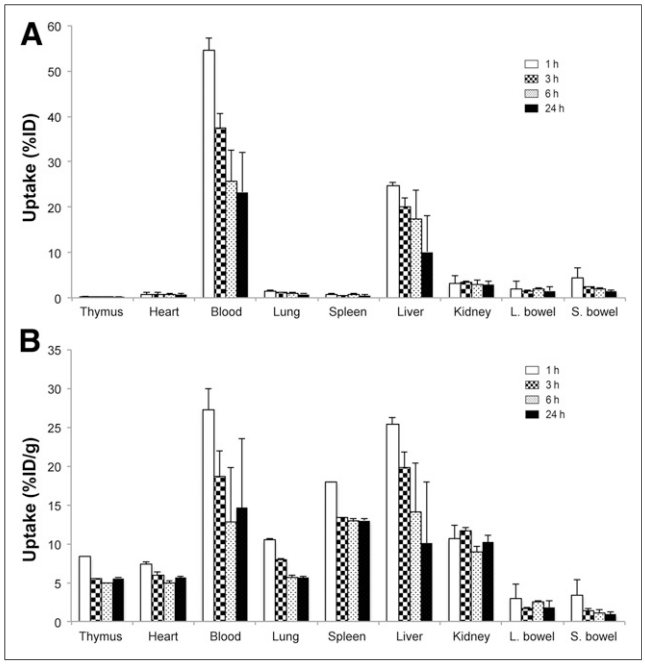

FIGURE 3. Biodistribution of radiolabeled anti-CD56 mAb at 1, 3, 6, and 24 h in normal mice. Data are percentage injected dose per organ (A) and percentage injected dose per gram (B). Error bars denote SD.

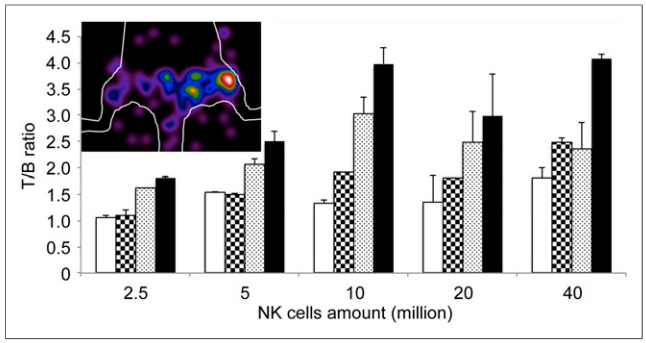

FIGURE 4. T/B ratios calculated in mice injected with increasing amounts of $CD56^+$ NKs in right thigh and with same amounts of $CD56^-$ control cells in left thigh. Mice were imaged at 1 h (white bar), 3 h (squared bar), 6 h (dotted bar), and 24 h (black bar). Image of mouse injected with 10^6 NK was acquired 24 h after injection of 5.5 MBq of radiolabeled mAb.

cells and the number of TINKs in the tumor. Overall, larger tumors were more infiltrated and showed more necrosis.

DISCUSSION

In the present study, we radiolabeled an anti-CD56 mAb as a novel radiopharmaceutical to image TINKs. This approach could be important in the development of novel cancer-immunotherapy drugs aimed at increasing NK infiltration into tumors, to follow up the efficacy of these drugs. Indeed, this approach could allow researchers to monitor cell trafficking directly in vivo. Despite the long half-life of mAbs, we chose ^{99m}Tc as the isotope because this anti-CD56 showed high-affinity binding in vitro and gave good visualization of TINKs in vivo within 3 and 24 h after intravenous administration. The mAb was radiolabeled using a well-established technique based on the use of S-HYNIC as a bifunctional

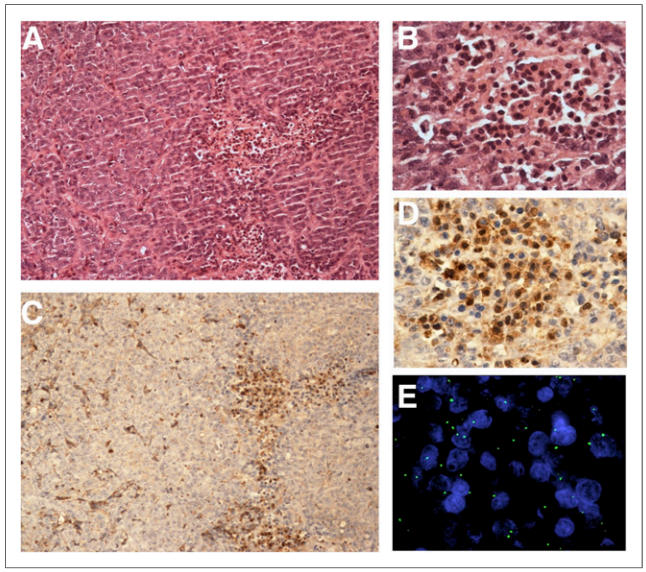

FIGURE 5. (A and B) Hematoxylin- and eosin-stained low-power (A) and high-power (B) fields showing tumor infiltrated by numerous lymphocytes. (C and D) Lymphocytic infiltrate was formed by NKs as demonstrated by CD57 immunostaining (brown cells). (E) They were from donor female subject (and therefore not from mouse host) as demonstrated by absence of Y chromosome detected by FISH analysis only in cancer cells from male donor (light green dots).

chelator obtaining a high labeling efficiency and stability. In vivo, in SCID mice lacking human NKs, the proposed radiopharmaceutical showed typical characteristics of other radiolabeled mAbs but with a shorter circulating half-life and high uptake in the liver and at a lower extent in the kidneys. After reconstitution of mice with human NKs, the biodistribution of the labeled antibody changed, showing a lower circulating half-life and higher liver and spleen activity due to specific binding to NKs homing in these tissues. These data are in agreement with those reported by Rai et al. (*24*) that hypothesized that either NKs could be resident in the liver or the organ itself could be responsible for the metabolization of both radiopharmaceutical and cells. In vivo targeting of Matrigel-immobilized NKs reached the maximum T/B ratio at between 6 and 24 h, suggesting that this time frame is the best choice for imaging. In our in vivo studies, we demonstrated a rapid infiltration of tumors by NKs starting as early as 3 h after intravenous administration of cells without any contamination from endogenous NKs, as revealed by immunohistochemistry and FISH staining. We can therefore speculate that murine NKs (present in SCID mice) do not efficiently recognize and infiltrate human xenograft tumors. The number of TINKs correlated positively with tumor size and with percentage necrosis over time, highlighting a direct killing effect of TINKs on the lesion and the full functionality of these cells. Imaging experiments on mice bearing ARO xenografts demonstrated a clear uptake of the radiopharmaceutical, with a T/B of 6.02 at 24 h. Moreover, tumor size, together with number of TINKs, positively correlated also with the radioactivity detected by ex vivo counting and by in vivo high-resolution portable mini γ camera imaging. This clearly indicates that it is possible to image TINKs in vivo with ^{99m}Tc-anti-CD56. Our study also opens the possibility of improving the described imaging technique using a positron-emitting isotope.

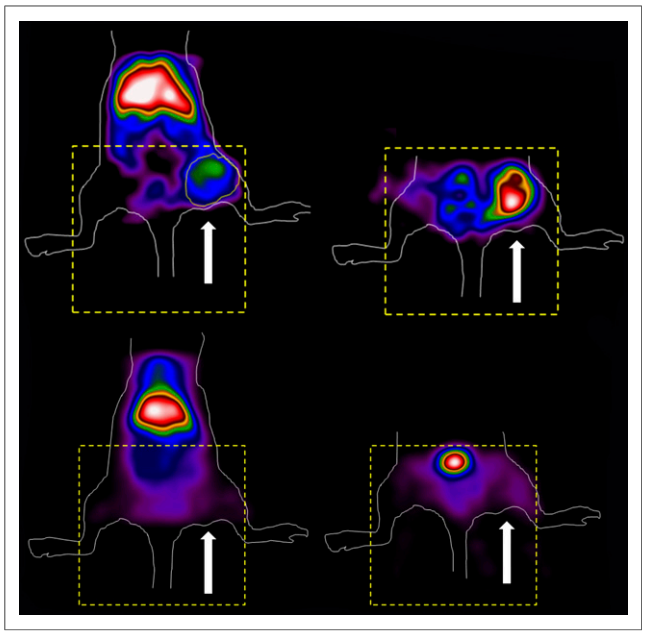

FIGURE 6. (Top) Total-body (left) and particular (right) scans of mouse bearing ARO xenograft (arrow) in right thigh. Animal intravenously received 10^6 human NKs and, after 24 h, 5.5 MBq of radiolabeled anti-CD56. Images were acquired at 24 h after injection of the radiopharmaceutical. (Bottom) As a negative control, mice bearing ARO xenograft intravenously received only radiolabeled antibody. Images were acquired at 24 h after injection. Each mouse is representative of group of 3 mice.

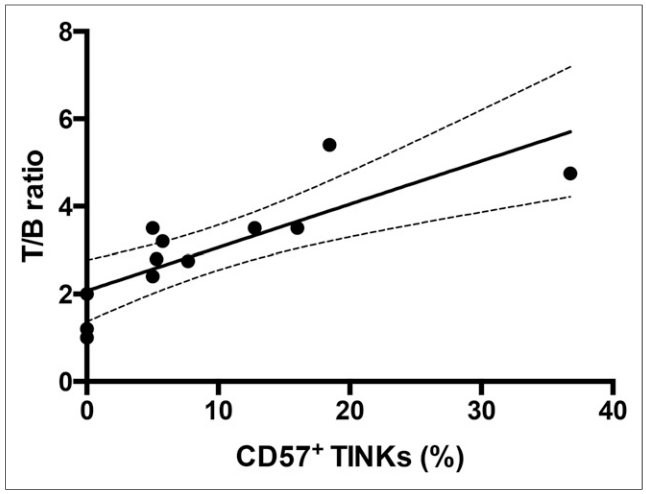

FIGURE 7. Correlation between TINKs in ARO tumors and calculated T/B ratio at 6 h ($P = 0.005$). Target was calculated over tumor, and background was calculated in similar-sized region over contralateral thigh. Percentage of $CD57^+$ NKs in tumors correlates with acquired radioactivity, indicating that radiolabeled anti-CD56 is able to specifically bind in vivo to $CD56^+/CD57^+$ NKs as revealed by both trafficking and immunohistochemistry studies. Line is linear regression fit of all points ($y = 0.098x + 2.0877$; $R^2 = 0.65433$).

Indeed, other attempts at imaging NKs have been reported in the literature, including MR imaging (*25*), fluorescence and bioluminescence imaging (*26*), SPECT (*27*), and PET (*28*). No technique has emerged as superior to the others, but nuclear medicine approaches have proven to be most promising for human studies.

To this aim, human NKs have been labeled ex vivo with ^{111}In-oxine and readministered to patients with metastatic melanoma (*29*). Interesting but preliminary results were also reported for patients with renal or colon carcinoma (*30,31*). Nevertheless, authors have reported that ^{111}In-oxine may have detrimental effects on NKs and is rapidly released from labeled cells, thus increasing background activity. Our approach overcomes these limitations and proved to be suitable for NK imaging in vivo, with no toxicity to cells. A limitation of our work is certainly the mouse model, which may not reflect the situation in humans. Indeed, our SCID mice were reconstituted with a supraphysiologic amount of human NKs and they rapidly infiltrated the human xenograft. In humans, the number of NKs infiltrating a tumor, or its metastasis, may be much lower than in our experiments, particularly under basal conditions. Many drugs already commercially available may, however, significantly increase the number of TINKs, thus allowing their in vivo detection.

CONCLUSION

This pilot study demonstrated that it is possible to efficiently image NKs in vivo and their trafficking in human tumors implanted in immune-deficient mice. Further studies are needed to confirm the application of this technique to monitor the efficacy of different therapeutic strategies aimed at increasing NK recruitment in tumors.

DISCLOSURE

The costs of publication of this article were defrayed in part by the payment of page charges. Therefore, and solely to indicate this fact, this article is hereby marked "advertisement" in accordance

with 18 USC section 1734. This work was supported by grants from the Italian Association for Cancer Research (AIRC IG-13234 and AIRC 5xmille) and by "Sapienza" University research projects. We also acknowledge the nonprofit association Nuclear Medicine Discovery for support. No other potential conflict of interest relevant to this article was reported.

REFERENCES

1. Catchpole B, Gould SM, Kellett-Gregory LM, Dobson JM. Immunosuppressive cytokines in the regional lymph node of a dog suffering from oral malignant melanoma. *J Small Anim Pract.* 2002;43:464–467.
2. Becknell B, Caligiuri MA. Interleukin-2, interleukin-15, and their roles in human natural killer cells. *Adv Immunol.* 2005;86:209–239.
3. Ma HL, Whitters MJ, Konz RF, et al. IL-21 activates both innate and adaptive immunity to generate potent antitumor responses that require perforin but are independent of IFN-gamma. *J Immunol.* 2003;171:608–615.
4. Baxevanis CN, Perez SA, Papamichail M. Cancer immunotherapy. *Crit Rev Clin Lab Sci.* 2009;46:167–189.
5. Cheng M, Chen Y, Xiao W, Sun R, Tian Z. NK cell-based immunotherapy for malignant diseases. *Cell Mol Immunol.* 2013;10:230–252.
6. Imai K, Matsuyama S, Miyake S, Suga K, Nakachi K. Natural cytotoxic activity of peripheral-blood lymphocytes and cancer incidence: an 11-year follow-up study of a general population. *Lancet.* 2000;356:1795–1799.
7. Coca S, Perez-Piqueras J, Martinez D, et al. The prognostic significance of intratumoral natural killer cells in patients with colorectal carcinoma. *Cancer.* 1997;79:2320–2328.
8. Jin J, Fu B, Mei X, et al. $CD11b^{-}CD27^{-}$ NK cells are associated with the progression of lung carcinoma. *PLoS One.* 2013;8:e61024.
9. Kalinski P, Giermasz A, Nakamura Y, et al. Helper role of NK cells during the induction of anticancer responses by dendritic cells. *Mol Immunol.* 2005;42:535–539.
10. Meller B, Frohn C, Brand JM, et al. Monitoring of a new approach of immunotherapy with allogenic ^{111}In-labelled NK cells in patients with renal cell carcinoma. *Eur J Nucl Med Mol Imaging.* 2004;31:403–407.
11. Galli F, Histed S, Aras O. NK cell imaging by in vitro and in vivo labelling approaches. *Q J Nucl Med Mol Imaging.* 2014;58:276–283.
12. Signore A, Sensi M, Pozzilli C, Negri M, Lenzi GL, Pozzilli P. Effect of unlabeled indium oxine and indium tropolone on the function of isolated human lymphocytes. *J Nucl Med.* 1985;26:612–615.
13. Signore A, Beales P, Sensi M, Zuccarini O, Pozzilli P. Labelling of lymphocytes with indium 111 oxine: effect on cell surface phenotype and antibody-dependent cellular cytotoxicity. *Immunol Lett.* 1983;6:151–154.
14. Pozzilli P, Signore A, Pozzilli C. Detrimental effect of indium-111 on human-lymphocytes [letter]. *J Nucl Med.* 1984;25:830.
15. Zarcone D, Viale O, Cerruti G, et al. Antibodies to adhesion molecules inhibit the lytic function of MHC-unrestricted cytotoxic cells by preventing their activation. *Cell Immunol.* 1992;143:389–404.
16. Corsetti F, Chianelli M, Cornelissen B, et al. Radioiodinated recombinant human TSH: a novel radiopharmaceutical for thyroid cancer metastases detection. *Cancer Biother Radiopharm.* 2004;19:57–63.
17. Perussia B, Ramoni C, Anegon I, Cuturi MC, Faust J, Trinchieri G. Preferential proliferation of natural killer cells among peripheral blood mononuclear cells cocultured with B lymphoblastoid cell lines. *Nat Immun Cell Growth Regul.* 1987;6:171–188.
18. Stabile H, Carlino C, Mazza C, et al. Impaired NK-cell migration in WAS/XLT patients: role of Cdc42/WASp pathway in the control of chemokine-induced beta2 integrin high-affinity state. *Blood.* 2010;115:2818–2826.
19. Hjorth R, Jonsson AK, Vretblad P. A rapid method for purification of human granulocytes using Percoll: a comparison with dextran sedimentation. *J Immunol Methods.* 1981;43:95–101.
20. Lindmo T, Boven E, Cuttitta F, Fedorko J, Bunn PA Jr. Determination of the immunoreactive fraction of radiolabeled monoclonal antibodies by linear extrapolation to binding at infinite antigen excess. *J Immunol Methods.* 1984;72:77–89.
21. Laemmli UK. Cleavage of structural proteins during the assembly of the head of bacteriophage T4. *Nature*. 1970;227:680–685.
22. Björke H, Andersson K. Automated, high-resolution cellular retention and uptake studies in vitro. *Appl Radiat Isot.* 2006;64:901–905.
23. Soluri A, Massari R, Trotta C, et al. New imaging probe with crystals integrated in the collimator's square holes. *Nucl Instr Meth Phys Res A.* 2005;554:331–-339.
24. Rai A, Chakravarty AK. Homing of radiolabelled recombinant interleukin-2 activated natural killer cells and their efficacy in adoptive immunotherapy against murine fibrosarcoma. *J Biosci.* 2007;32:1299–1305.
25. Sheu AY, Zhang Z, Omary RA, Larson AC. MRI-monitored transcatheter intra-arterial delivery of SPIO-labeled natural killer cells to hepatocellular carcinoma: preclinical studies in a rodent model. *Invest Radiol.* 2013;48:492–499.
26. Edinger M, Cao YA, Verneris MR, Bachmann MH, Contag CH, Negrin RS. Revealing lymphoma growth and the efficacy of immune cell therapies using in vivo bioluminescence imaging. *Blood.* 2003;101:640–648.
27. Jha P, Golovko D, Bains S, et al. Monitoring of NK-cell immunotherapy using non-invasive imaging modalities. *Cancer Res.* 2010;70:6109–6113.
28. Melder RJ, Brownell AL, Shoup TM, Brownell GL, Jain RK. Imaging of activated natural killer cells in mice by positron emission tomography: preferential uptake in tumors. *Cancer Res.* 1993;53:5867–5871.
29. Schäfer E, Dummer R, Eilles C, et al. Imaging pattern of radiolabelled lymphokine-activated killer cells in patients with metastatic malignant melanoma. *Eur J Nucl Med.* 1991;18:106–110.
30. Matera L, Galetto A, Bello M, et al. In vivo migration of labeled autologous natural killer cells to liver metastases in patients with colon carcinoma. *J Transl Med.* 2006;4:49.
31. Meller B, Frohn C, Brand JM, et al. Monitoring of a new approach of immunotherapy with allogenic ^{111}In-labelled NK cells in patients with renal cell carcinoma. *Eur J Nucl Med Mol Imaging.* 2004;31:403–407.